Center for Astrophysics

Harvard College Observatory
Smithsonian Astrophysical Observatory

MEMORANDUM

September 24, 1998

To: M. Zombeck

From: Almus Kenter,Gary Meehan

Subject: HRC QE Versus Angle of Incidence

1 Introduction

The quantum efficiency of MCPs depends strongly on the angle of the incident flux of radiation with respect to to the MCP pore angles. Since this angular QE dependence is due to absorption and grazing reflection down the pores, it is affected by pore coating, surface finish and X-ray energy.

Previous work and analysis has shown that given the range of AXAF cone angles, CsI coated input MCPs with bias angles of $\sim 6°$ have one major benefit. This benefit is a combination of better overall Effective Area (EA) for the HRMA/HRC and less variation over the range of AXAF cone angles.

The downside to the $\sim 6°$ bias angle MCPs is that the vacuum deposition process we have employed does not uniformly coat the walls of the MCP pores. As a result there is an azimuthal dependence of photocathode coating and a resulting azimuthal dependence of QE. 0° bias input MCPs such as used on the Einstein and ROSAT, are by definition azimuthally symmetric, aesthetically pleasing but not necessarily optimium for AXAF.

We have been investigating the angular dependence of the quantum efficiency of coated HRC type MCPs. These investigations are intended to provide data products to those trying to better understand and refine the HRC final calibration.

This information will be of particular interest and use to those applying flat field HRC QE values to grating data, EA measurements, off-axis response and High Energy Supression Filter (HESF) data.

Previous measurements have been done to investigate and quantify these effects however in most cases these previous investigations were limited in the number of energies and range of angles.

Using a soft X-ray monochromator (McPherson 1 meter VUV scanning monochromator), and two orthogonal rotary stages, the QE versus angular dependence of HRC type detectors has been investigated over a large set (~ 10) energies and a large set of angles. The energies investigated were all $\leq$ 1487eV. These lower energies were most important as this is where the QE vs angle effect is largest and where the HRMA "effective cone angle" (relative contribution from outer-most shell) is largest. The scanned angles were chosen to cover the important AXAF range and mimic the values of the actual average HRMA shell cone angles.

This preliminary report discusses analysis and results using both HRC-S (ie Philips mfg.) and HRC-I detector (GEOC mfg.) representative MCPs.

2 Applicability and Caveats

In flight, X-rays from the HRMA converge at the "cone"angles down to the size of the HRMA PSF ($\sim 50\mu$m). On such a small spatial scale, one would expect large variations in the detector uniformity, however in flight dithering will average out these variations in response over a much larger area.

In the laboratory, the effects of the cone angles and the averaging were performed by using two orthogonal rotary stages to recreate the effect of the AXAF angles and a large fraction of the detector was illuminated.

There are several caveats that one must consider in applying these results. These caveats stem primarily from the fact that we are using test items; we used flight-spare coated MCPs that we believe are representative of the actual flight HRC-I and HRC-S.

The MCPs were nominaly specified to have a $6°$ bias angle, though for the actual flight items, this was never verified.

Even though coating of the flight HRC MCPs and of these test MCPs was performed in the same coating deposition facility, using the same written procedure, by the same personel -differences do exist. The most obvious difference is that the final CsI coating thickness were different.

3 Laboratory Setup

3.1 Experminetal Setup

The laboratory aparatus consisted of the HRC $\sim$ 6m X-ray pipe. A McPherson 1 meter VUV scanning monochromator was mounted on the source end. During operation, no monitoring of the X-ray beam was performed for either temporal or spectral variation or content. Extensive previous experience with this source has shown that it is temporaly stable and spectrally pure.

The chevron pair of test MCPs were assembled into a laboratory HRC-I type MCP holder with an aluminized polypropylene shield. The MCP assembly was incorporated with a laboratory version 10 kΩ Crossed Grid Charge Detector (CGCD). The resulting detector was placed on a two axis rotary stage in the HRC test chamber. During assembly,transport and configuration, the test detector was continuously kept in a dry nitrogen atmosphere to protect the photo-cathode.

The stages were configured to ensure that the axes of motion passed through the center of the front surface of the input MCP. The two rotary stages were New England Affiliated Technology (NEAT) models RT-10-SM and RT-6-SM . The motion of the stages was under computer/software control. The two stage system was mounted to a cast aluminum alignment plate inside the test chamber. The two axes are the "tilt" angle θ and the azimuthal angle ϕ. The motion control set-up is depicted in Figure 1. The range of the θ scan ($27°$) and the orientation of the scan with respect to the pore bias is depicted in Figure 3. Figure 3 also depicts the location of the HESF for the HRC-S.

The flight HRC focal plane layout is depicted in Figure 2; it indicates the orientation of the pore bias angles with respect to the spacecraft and detector coordinates.

Data acquisition was done with a laboratory version of the HRC electronics (Unit I) that was specifically modified to keep track of the motion control.

Data was analyzed off-line.

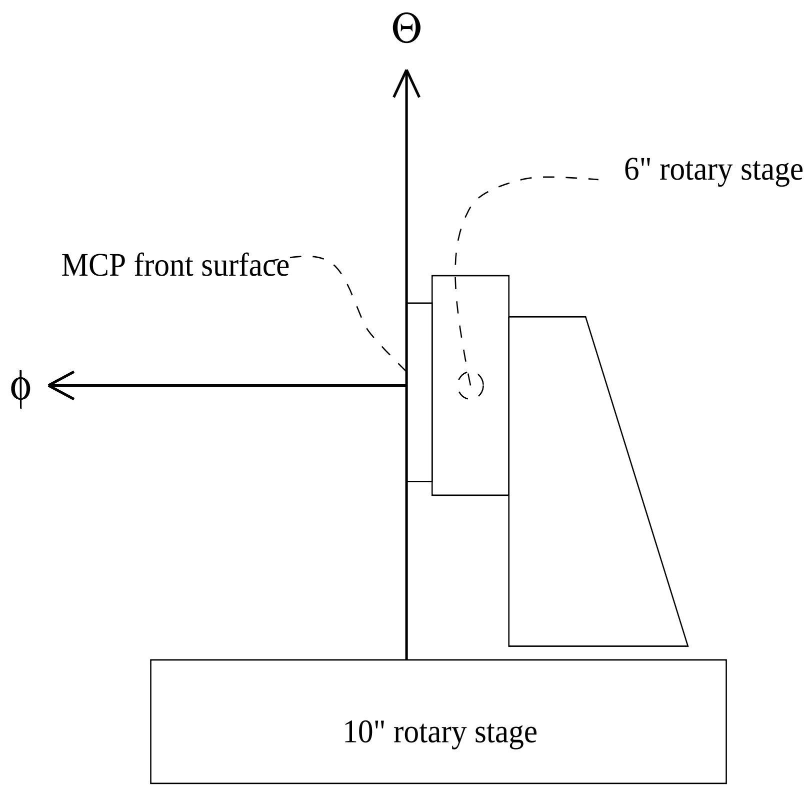

Figure 1: Stages used for measuring QE versus angle of X-ray incidence. Rotation axes were engineered to go through the center and face of the input MCP. The two axes, θ and ϕ are as indicated

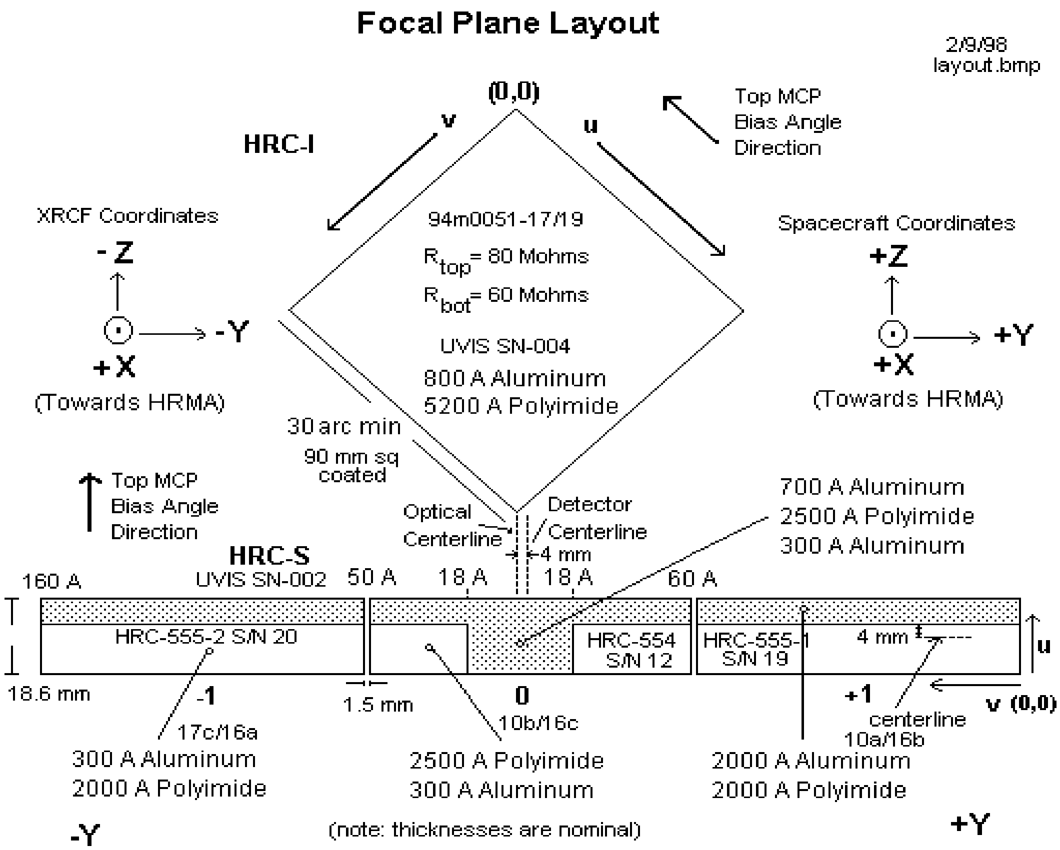

Figure 2: Layout of the HRC focal plane. The MCP pore angle orientations are as indicated; note that for the HRC-S the pore angles are perpendicular to the dispersion direction and tilting away from the High Energy Suppression Filter (HESF).

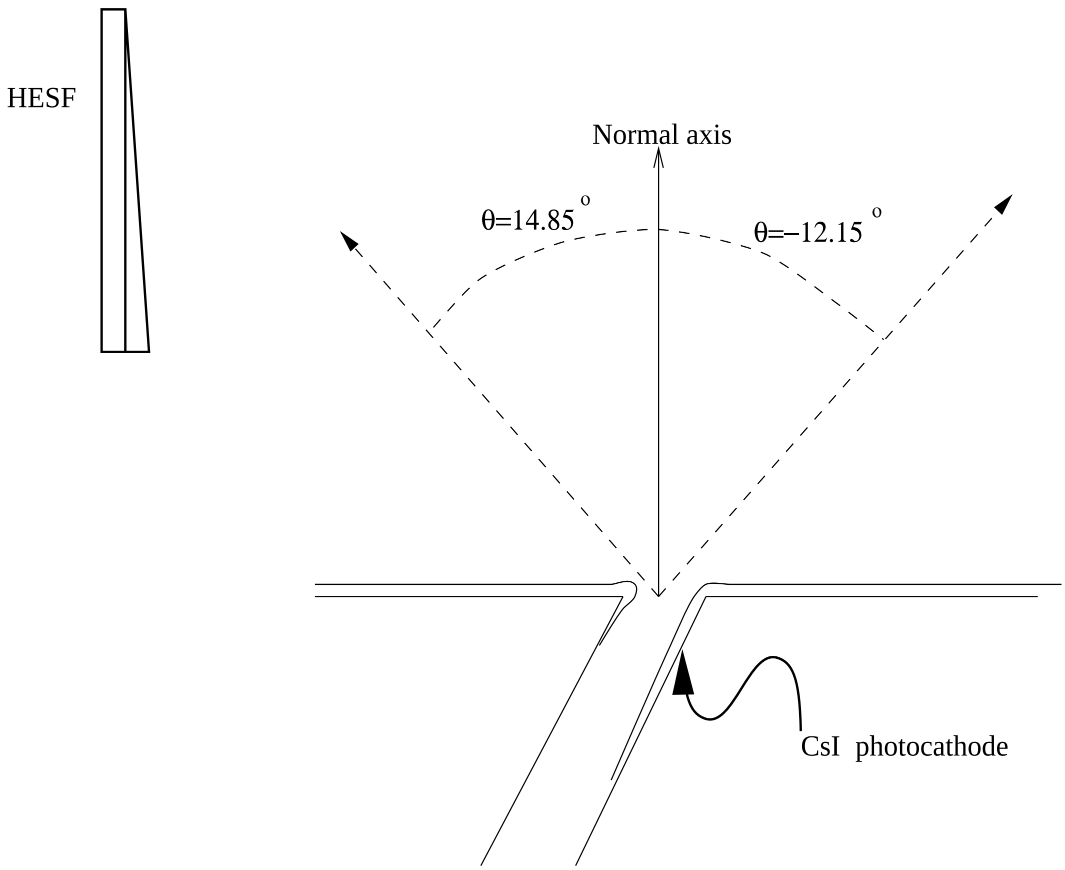

Figure 3: Range of theta scan with respect to pore bias angle. X-rays reflected from High Energy Suppression Filter (HESF) would come from the positive theta direction. Dimensions are for illustration purposes only.

3.2 Components

Both HRC detectors (HRC-S and HRC-I) consist of pairs of MCPs in a chevron configuration. Each chevron pair consists of two MCPs with a 6° (nominal) bias angle. The front surface of the input MCPs of both detectors were coated with a CsI photocathode to enhance the QE over the AXAF band.

The HRC-I type MCPs were manufactured by the Galileo Electro Optics Corp. (GEOC). They are 100mm x100mm in size, they have 10 μm pores on 12.5 μm centers. and they have a nominal 120: L/D ratio - they are 1.2mm thick. The MCPs were nominaly specified to have a 6° bias angle, though this was never verified. The actual flight HRC-I MCPs are serial #s GEOC 94m0051-17 (input) and GEOC 94m0051-19 (output). The input MCP was coated at the SAO coating deposition facility according to procedure SAO-HRC-PROC-95-165. The final coating thickness as determined by witness sample was $1,440\AA$.

The HRC-S type MCPs were manufactured by Philips Components. They have 12 μm pores on 15 μm centers. They have a nominal 120: L/D ratio - they are 1.5mm thick. Philips MCPs were nominaly specified to have a 6° bias angle, though this was never verified for the actual flight items. The flight HRC-I MCPs are serial numbers: NH002- 10-a, 10-b, 17-c (input) and 16-b, 16-c, 16-a (output). The input MCPs was coated at the SAO coating deposition facility according to procedure SAO-HRC-PROC-95-165. The final coating thickness as determined by witness sample was $1,400\AA$

Test article MCPs were selected from our limited selection of flight spares. Both HRC-S and HRC-I test MCPs were 100mm $\times$ 100mm format. The test item input MCPs had CsI coatings of $1,875\AA$ for the Philips (HRC-S) and unknown thickness ($1,500\AA$?) for the GEOC (HRC-I).

4 The Measurements

The first measurement determined the MCP bias angle by exposing the detector to 1487eV X-rays from the monochromator and scanning through the θ angle. The QE versus theta angle curve was then used to determine the MCP bias angle as the position of the $\theta = 0°$ (normal incidence) was known from the mechanical setup.

This measurement confirmed the 6° bias angle for the Philips (HRC-S type) MCPs. In contrast, similar analysis shows that the GEOC MCPs (HRC-I type) have a bias angle of only 4.7°

5 Tests and Data Products

Following the MCP bias angle determination, the detector was scanned in θ from $-12°$ to 15° with respect to normal incidence in 0.1° steps. Data integration times and rates were adjusted to ensure $\sim 2,000$ -$10,000$ events per data point.

This data set, presented in Figures 6 through Figure 19, shows the QE dropping to a minimum as the X-rays reflect/pass down the MCP pores. The relationship of critical angle versus energy is apparent from the width of the "dip" in QE; sharper at higher energies and broader at lower energies. In addition, it is apparent that the data is not symmetric about the QE "dip"; this is due to the azimuthal dependence of the CsI photocathode coating. On the low QE side of the QE dip, the X-rays are impinging on the sides of the MCP pores with minimum photocathode coating. On the high QE side of the QE dip, the X-rays are impinging on the sides of the MCP pores with maximum photocathode coating. (See Figure 4.) The GEOC MCPs, with the smaller pore angle, show greater symmetry about the QE-dip as would be expected. Furthermore, bare plates should and do show symmetry about the pore-bias angle; Figure 5 shows that the QE response is symmetrical about the pore

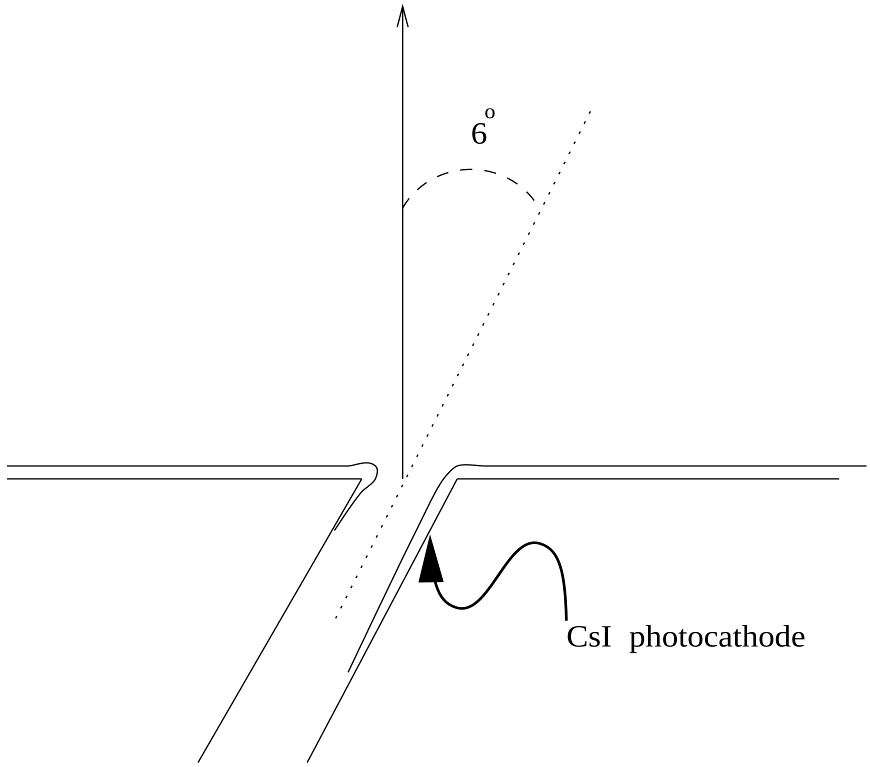

Figure 4: Coating asymmetry due to pore bias. Dimensions are for illustration purposes only. QE will not by symmetric about the pore angle due to the differing amounts of coated pore exposed.

axis; this proves that the QE asymmetry about the pore axis in coated plates is due to the asymmetry of the CsI coating.

The AXAF cone angles never see the “dark” side of the pores; they are limited to a small range of the QE versus theta curve as indicated in Figures 6 through Figure 11 Indicating the range of the HRMA cone angles on such a figure does not necessarily imply that these QE versus θ curves can represent the generalized QE variation with angle of X-ray incidence. The QE versus theta scans are limited in sampling the azimuthal dependence at only $\phi = 0$ and 180°. However as will be shown, this equivalence turns out to be a reasonable approximation over the limited range of the AXAF cone angles.

The second set of measurements were intended to simulate the AXAF-HRMA cone ge-

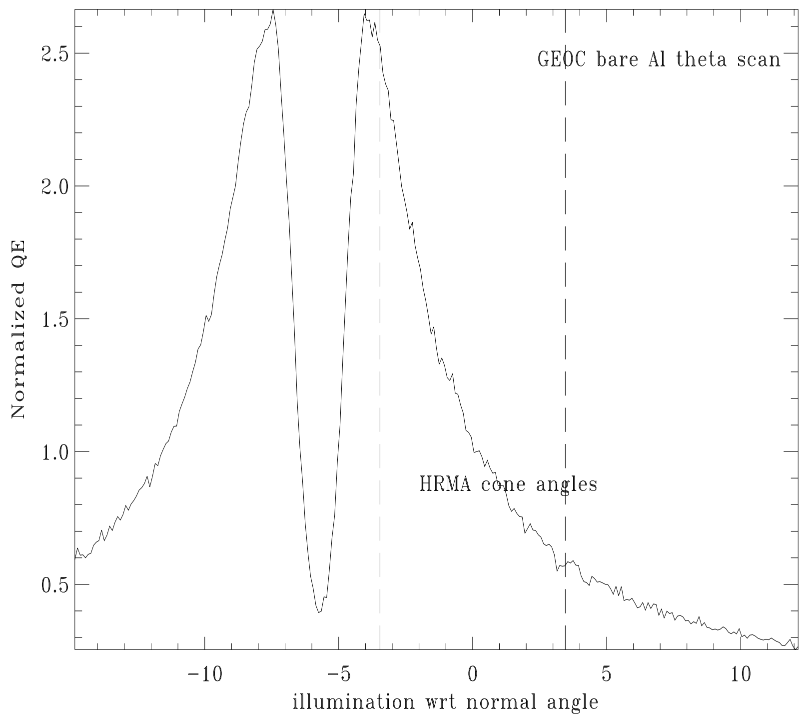

Figure 5: QE versus angle for bare GEOC MCPs. This data set shows that the QE asymmetry about the pore axis for coated MCPs is due to the asymmetry of the CsI coating. Note: these GEOC MCPs have bias angles of $\sim 6°$.

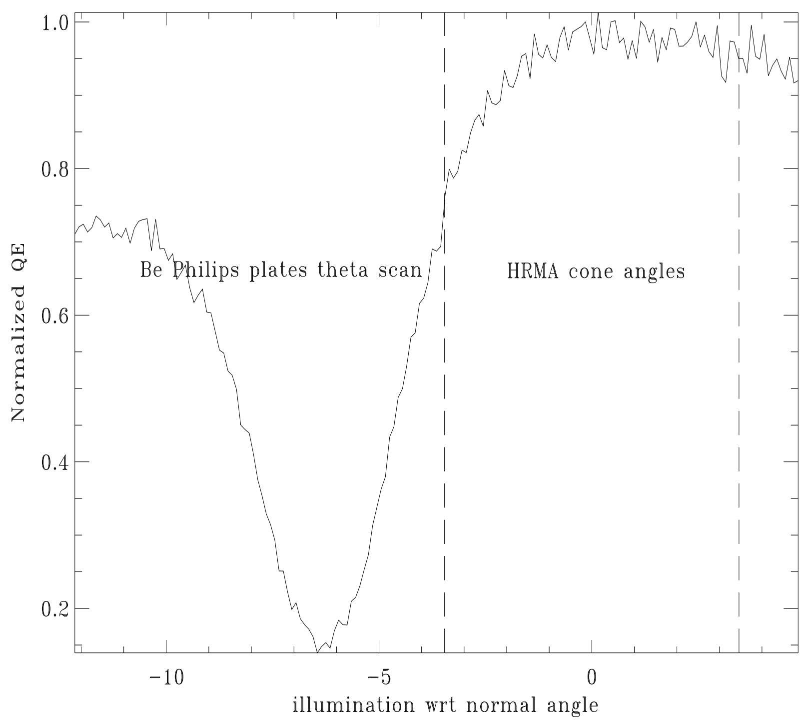

Figure 6: Relative QE versus θ at $E = 108.5$eV for HRC-S type MCPs. The range of the AXAF HRMA cone angles is indicated. QE values have been normalized so that $QE = 1$ at $\theta = 0°$

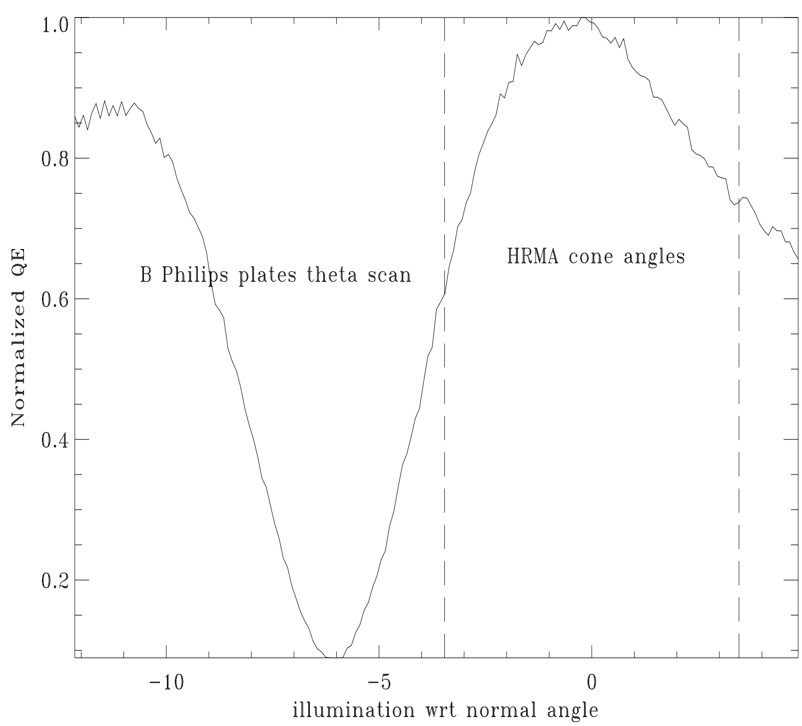

Figure 7: Relative QE versus θ at $E = 183.3$eV for HRC-S type MCPs.. The range of the AXAF HRMA cone angles is indicated. QE values have been normalized so that $QE = 1$ at $\theta = 0°$.

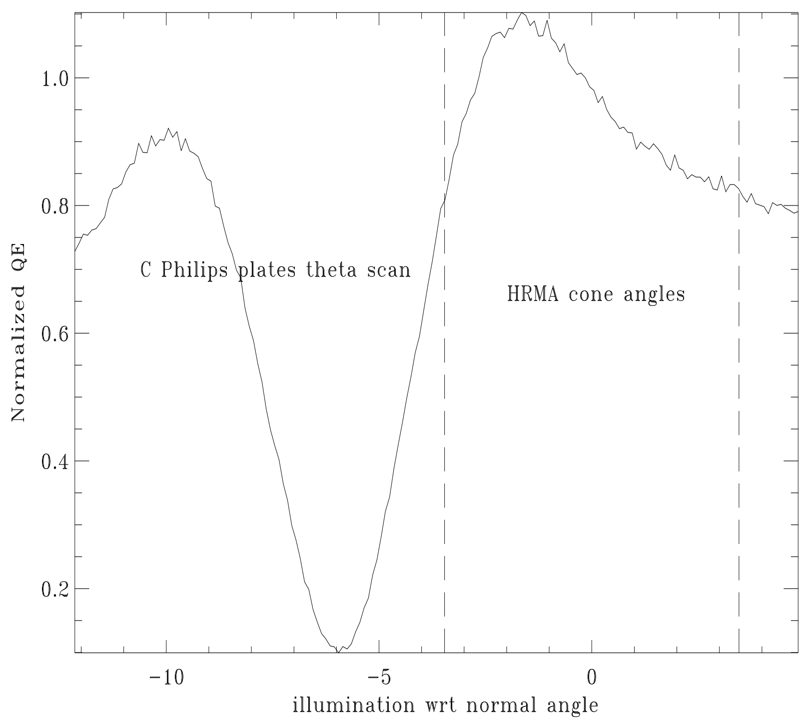

Figure 8: Relative QE versus θ at $E = 277.0$eV for HRC-S type MCPs.. The range of the AXAF HRMA cone angles is indicated. QE values have been normalized so that $QE = 1$ at $\theta = 0°$.

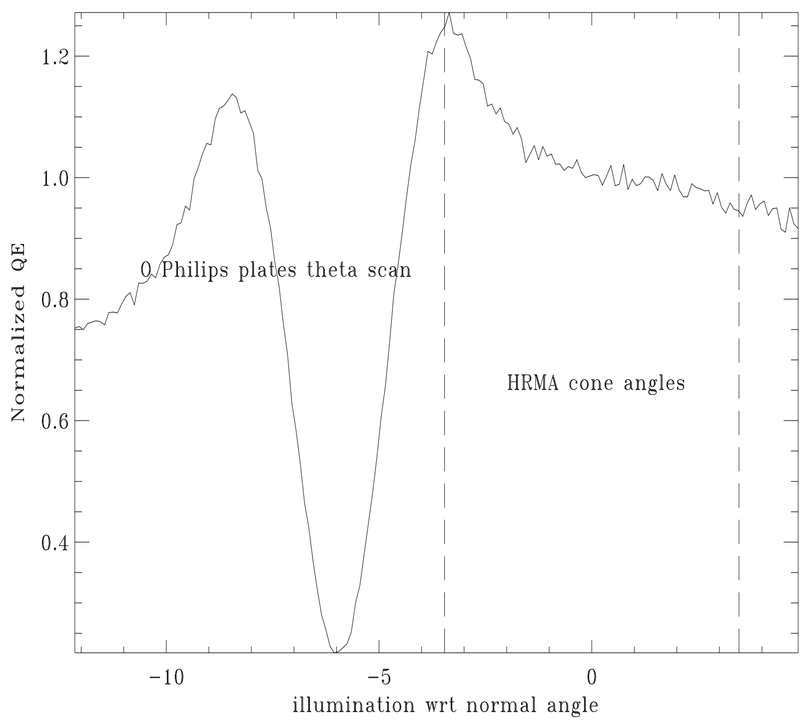

Figure 9: Relative QE versus θ at $E = 524.9$eV for HRC-S type MCPs.. The range of the AXAF HRMA cone angles is indicated. QE values have been normalized so that $QE = 1$ at $\theta = 0°$.

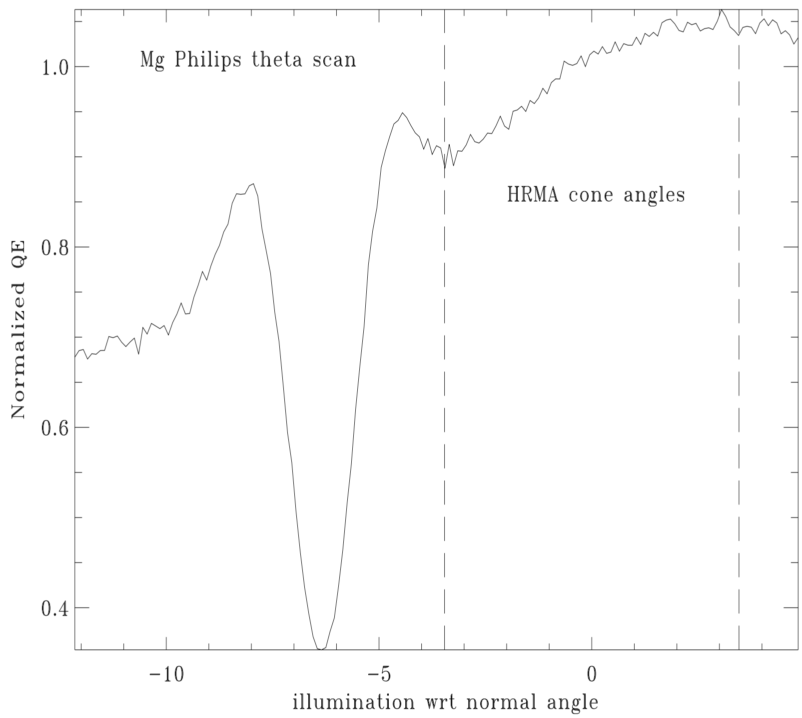

Figure 10: Relative QE versus θ at $E = 1253.6$eV for HRC-S type MCPs.. The range of the AXAF HRMA cone angles is indicated. QE values have been normalized so that $QE = 1$ at $\theta = 0°$.

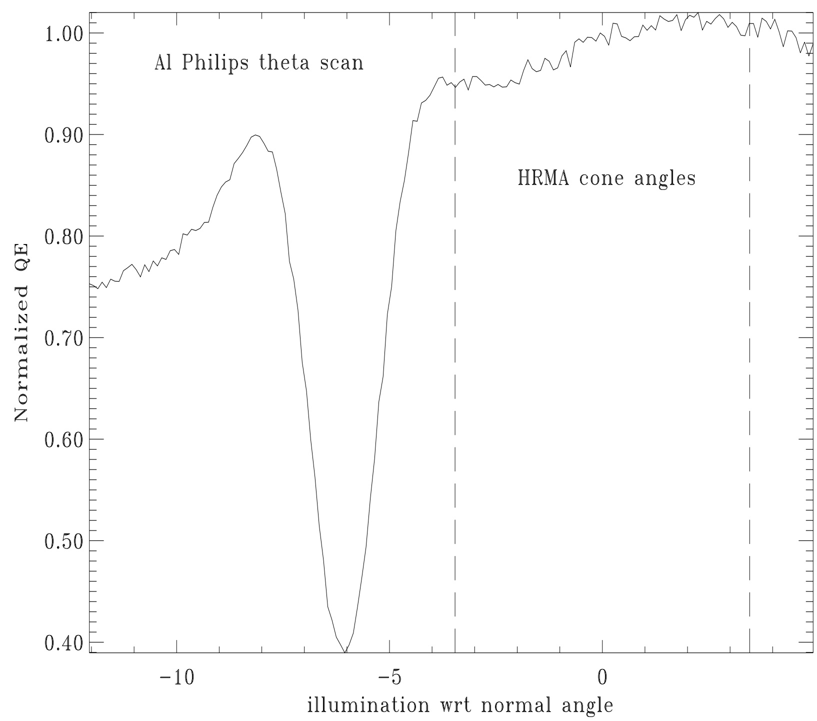

Figure 11: Relative QE versus θ at $E = 1486.7$eV for HRC-S type MCPs.. The range of the AXAF HRMA cone angles is indicated. QE values have been normalized so that $QE = 1$ at $\theta = 0°$.

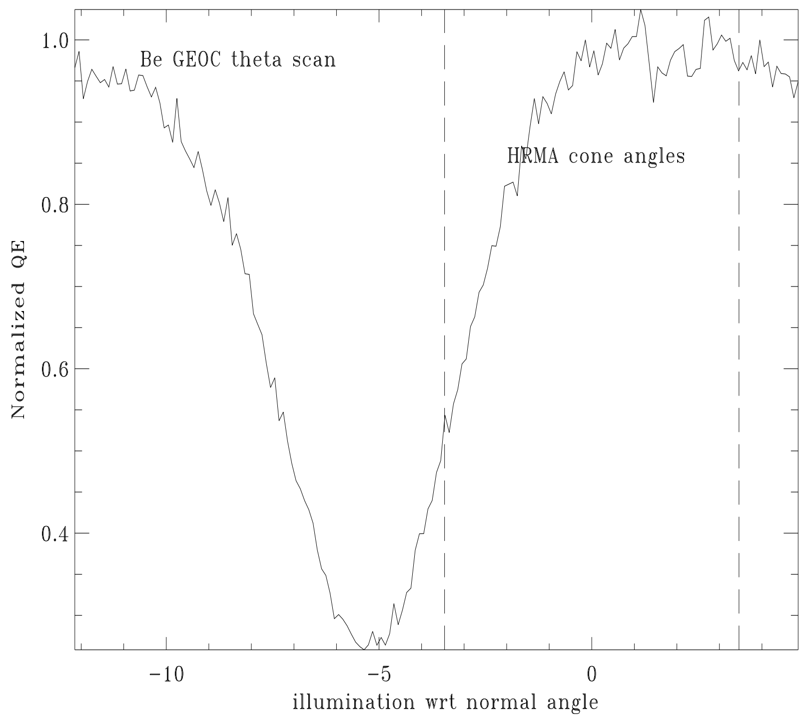

Figure 12: QE versus θ at $E = 108.5$eV for HRC-I type MCPs. The range of the AXAF HRMA cone angles is indicated. QE values have been normalized so that $QE = 1$ at $\theta = 0°$

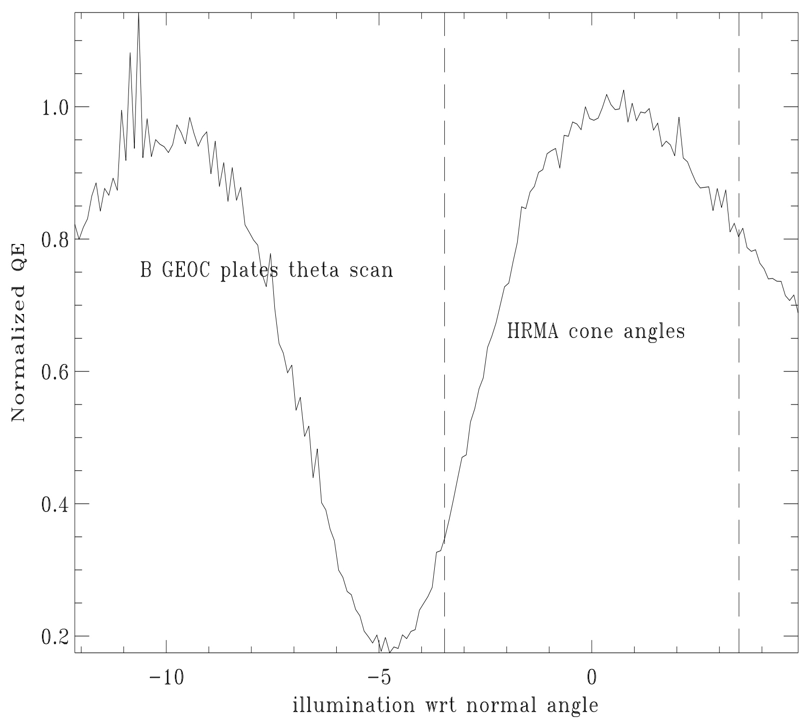

Figure 13: Relative QE versus θ at $E = 183.3$eV for HRC-I type MCPs. The range of the AXAF HRMA cone angles is indicated. QE values have been normalized so that $QE = 1$ at $\theta = 0°$.

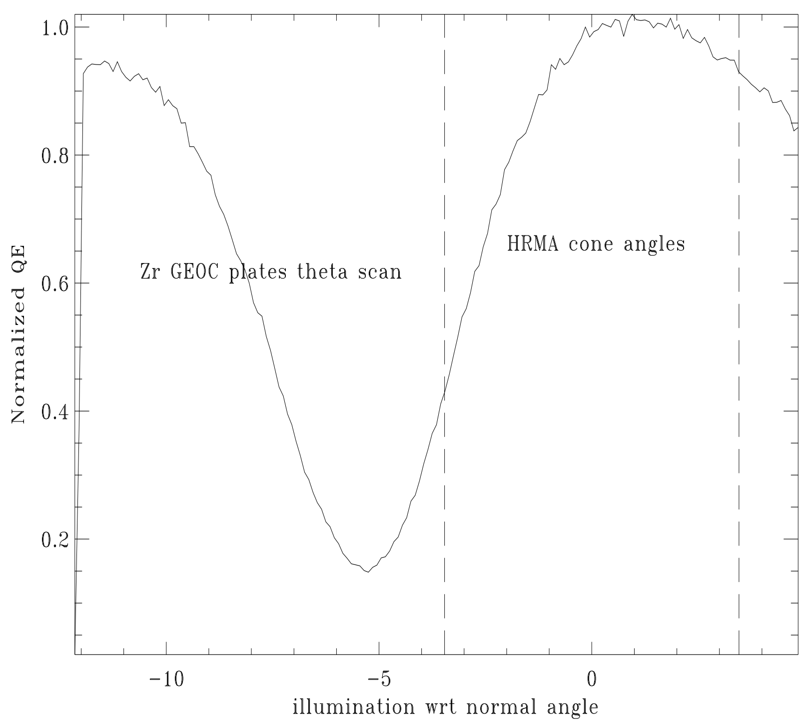

Figure 14: Relative QE versus θ at $E = 151.1$eV for HRC-I type MCPs. The range of the AXAF HRMA cone angles is indicated. QE values have been normalized so that $QE = 1$ at $\theta = 0°$. Glitch at $\sim -12°$ is not real and is due to operator error.

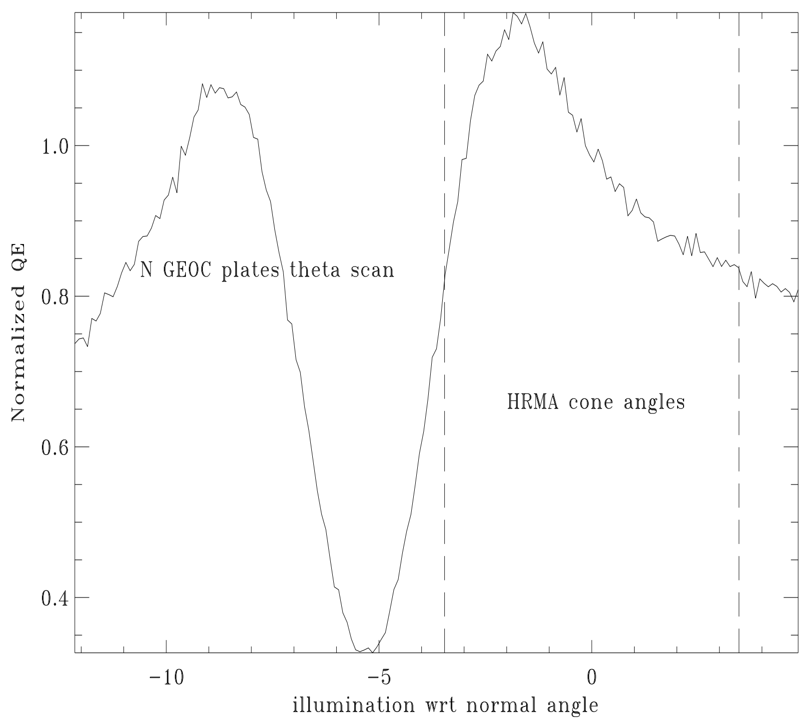

Figure 15: Relative QE versus θ at $E = 392.4$eV for HRC-I type MCPs. The range of the AXAF HRMA cone angles is indicated. QE values have been normalized so that $QE = 1$ at $\theta = 0°$.

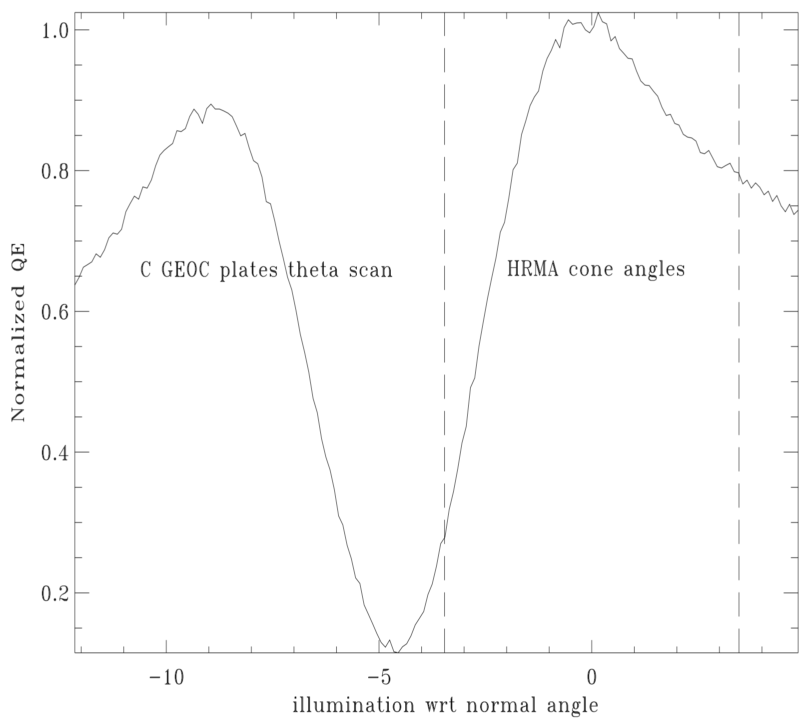

Figure 16: Relative QE versus θ at $E = 277.0$eV for HRC-I type MCPs. The range of the AXAF HRMA cone angles is indicated. QE values have been normalized so that $QE = 1$ at $\theta = 0°$.

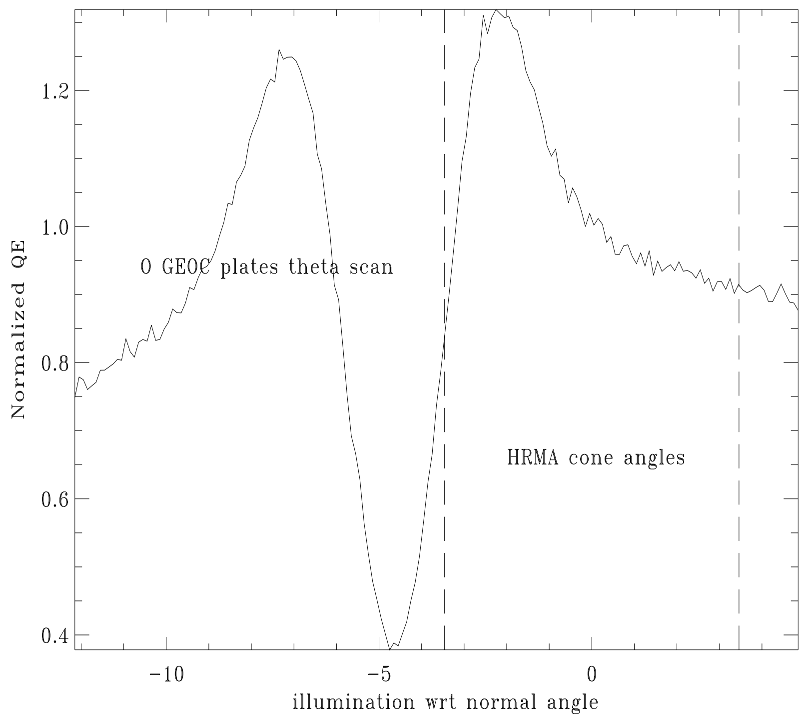

Figure 17: Relative QE versus θ at $E = 524.9$eV for HRC-I type MCPs. The range of the AXAF HRMA cone angles is indicated. QE values have been normalized so that $QE = 1$ at $\theta = 0°$.

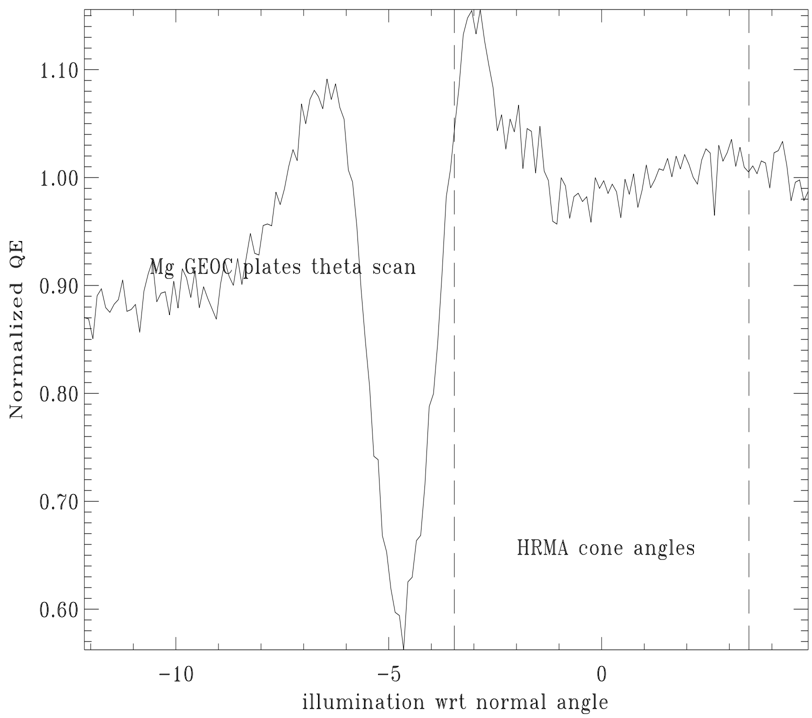

Figure 18: Relative QE versus θ at $E = 1253.6$eV for HRC-I type MCPs. The range of the AXAF HRMA cone angles is indicated. QE values have been normalized so that $QE = 1$ at $\theta = 0°$.

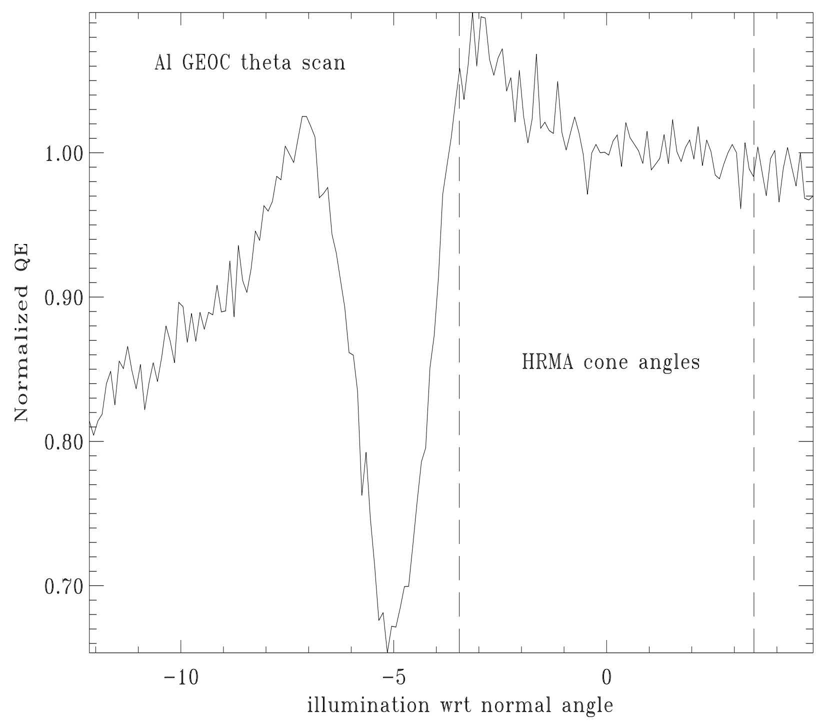

Figure 19: Relative QE versus θ at $E = 1486.7$eV for HRC-I type MCPs. The range of the AXAF HRMA cone angles is indicated. QE values have been normalized so that $QE = 1$ at $\theta = 0°$.

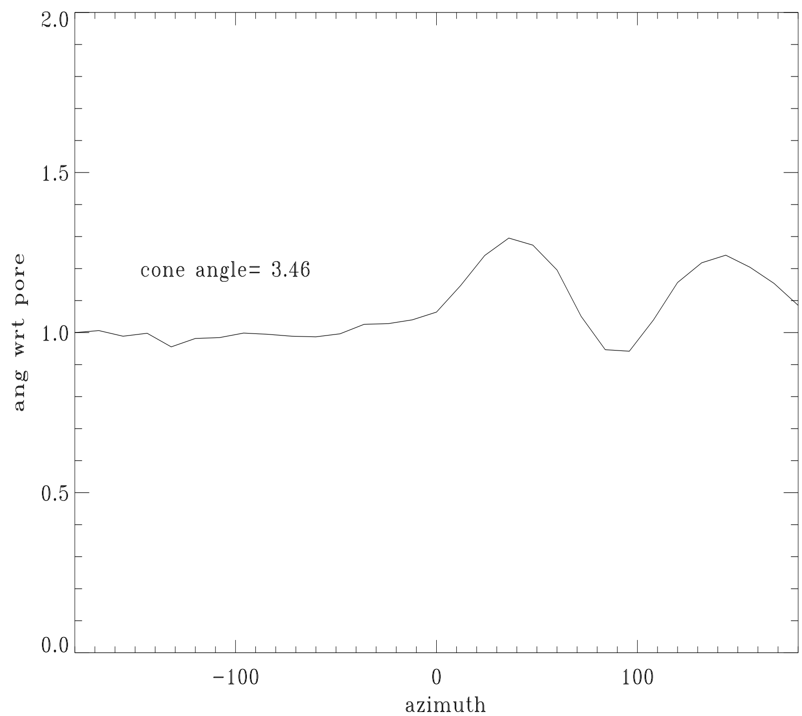

Figure 20: Laboratory measurement to determine relative QE for C X-rays (277eV) versus azimuth for outer-most HRMA shell. Structure is due to sampling within the broad dip in QE versus angle for C X-rays. (HRC-S type Philips MCPs).

ometry; the detector was first tilted in θ to + average cone angle. The detector was then scanned in ϕ from -180 to $0°$. The measurement was then repeated at $\theta = -$ average cone angle. These two measurements effectively scan the entire HRMA cone in azimuth. These measurements were repeated for all four of the HRMA average cone angles. Some representative QE versus ϕ measurements are shown in Figures 20 and 21.

Using the QE versus θ result, as a generalized QE versus angle "model" the expected response of the coated MCPs was determined by calculating the angle of incidence of X-rays with respect to the MCP pores as a function of cone angle and azimuth.

$$QE(\alpha) = QE(\Theta, \Phi)$$

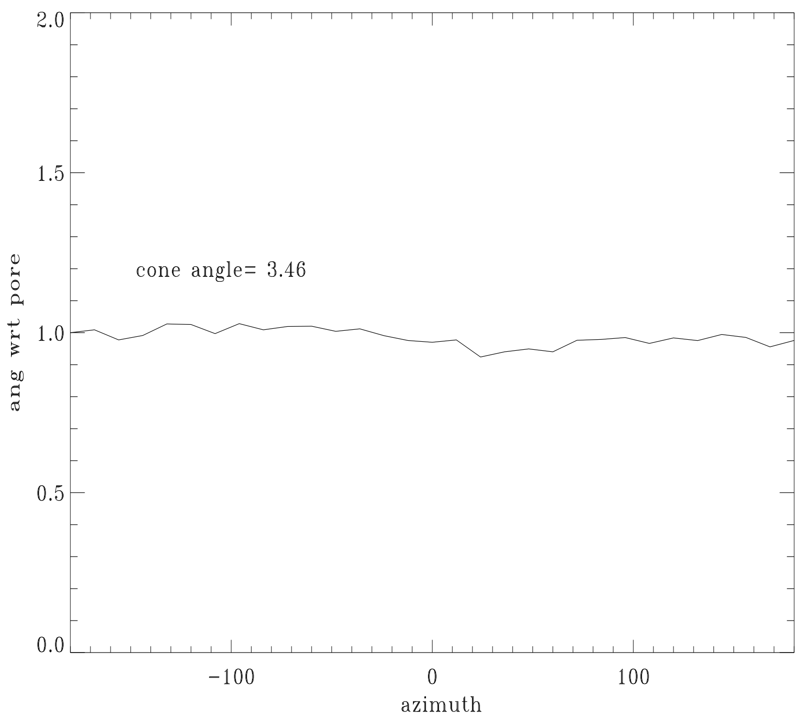

Figure 21: Laboratory measurement to determine relative QE for *Al* X-rays (1487eV)versus azimuth for outer-most HRMA shell. No structure is evident. (HRC-S type Philips MCPs)

This angle, α can be written as:

$$\alpha = cos^{-1}(\mathbf{p} \bullet \mathbf{C})$$

Where p is a unit vector in the direction of the MCP pores. C is a unit angle in the negative direction of the impinging X-rays. The angle between the pore channels and a X-ray from would then be:

$$\alpha = cos^{-1}(\mathbf{p} \bullet \mathbf{C})$$

Where

$$\mathbf{p} = sin(\omega)cos(\phi)\hat{x} + sin(\omega)sin(\phi)\hat{y} + cos(\omega)\hat{z}$$

and:

$$\mathbf{C} = sin(\theta)cos(\Phi)\hat{x} + sin(\theta)sin(\Phi)\hat{y} + cos(\theta)\hat{z}$$

The geometry of the angles involved is depicted in Figure 22.

The value of α (angle of X-ray incidence with respect to MCP pore axis) is depicted in Figure 23 for 6° bias MCPs.

Expected QE versus azimuth was calculated using $QE(\alpha)$ and the range of α as depicted in Figure 23. This result was compared with the laboratory HRMA cone angle scan for the outer-most shell. The comparison is presented in Figure 24. It is apparent that the QE versus angle data presented in Figure 6 through Figure 19 can be used to predict the entire angular QE dependence for the HRC over the range of the HRMA cone angles.

5.1 Application of Results

Two applications of the above data set are herein presented. Both sets of results are based on using QE versus θ as representative of the angular response of CsI coated MCPs.

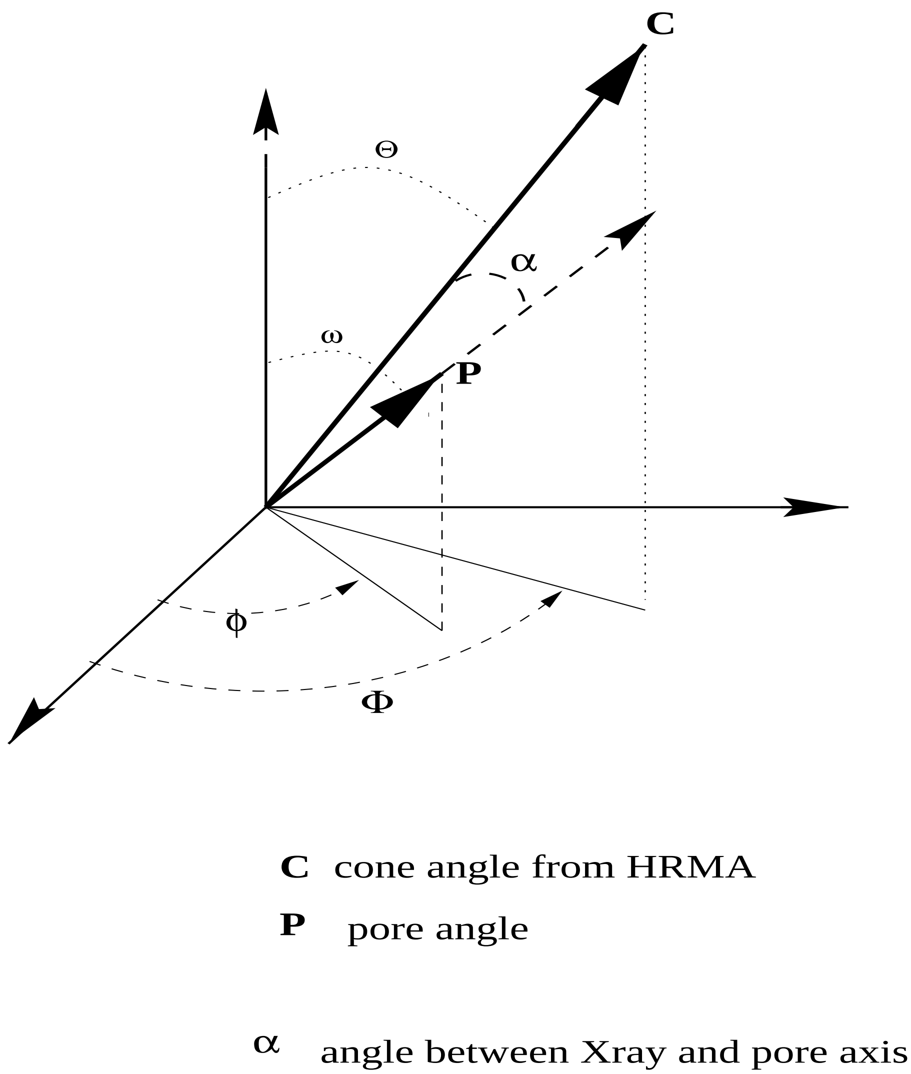

Figure 22: Geometry of pore angles and angle of X-ray incidence.

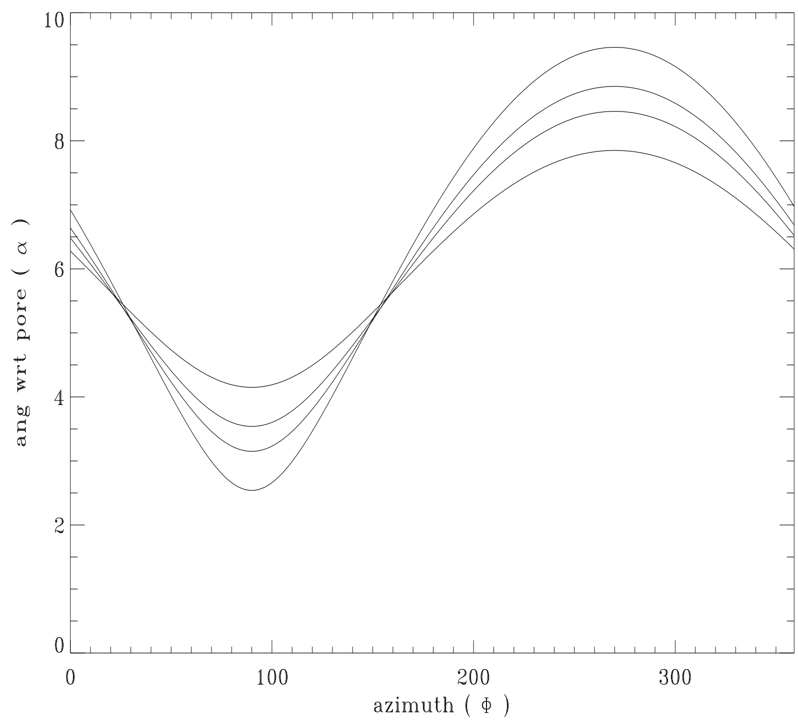

Figure 23: Angle of incidence of X-rays with respect to MCP pore from the four HRMA shells versus azimuth for a 6° bias MCP.

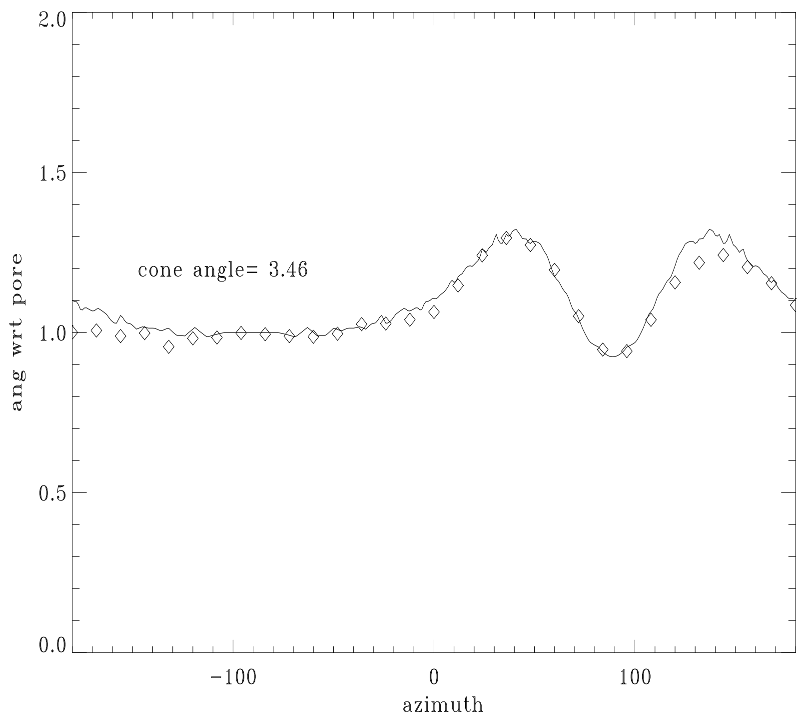

Figure 24: Comparison of scan in Φ with expected response using QE versus θ data as a "model". Statistical errors are $\sim 3\%$. Data from Philips MCPs, C (277eV) X-rays. Range of incident angles is as depicted in Figure 23.

5.2 Re-verifying the 6° bias Choice

Using the QE versus θ data sets, one can determine the pore angle bias which maximizes the HRMA/HRC Effective Area. $EA(E,\omega)$ i.e. the effective area versus MCP pore bias angle (ω) and Energy, E can now be calculated. The result

$$\sum_i^4 EA_i < QE_i(\omega) >$$

(in arbitrary units) is depicted in Figure 25. Where $< QE_i(\omega) >$ is the expected QE of the HRC appropriately averaged over incident angles from the i^{th} HRMA shell.

$$< QE_i(\omega) >= \int_0^{2\pi} QE(\theta_i, \phi) d\phi$$

EA_i is the effective area of the appropriate shell at the energy of interest, and θ_i is the cone angle of that particular shell.

As can be seen from Figure 25, the choice of 6° pore bias is about optimum.

5.3 Applying "flat field" results to HRMA EA values

Post XRCF, the HRC detectors were modified and a series of X-ray flat field illumination QE measurements were performed. In these measurements the HRC detectors were illuminated with X-rays from a Manson Model 5 electron impact source. Filters were used to improve the line to continuum ratio and the X-ray flux was measured with flow p roportional counters. The resultant absolute QE values were used as the basis for the "final" HRC QE and EA models.

The HRC team has repeatedly claimed that for higher energies ($\sim$ 1keV) that normal incidence flat field QE data are a good approximation of the QE of the detector when it is operated behind the HRMA. This claim has been verified using the above data sets. Such simple averaging,however, does not apply for lower energies. The net result is that

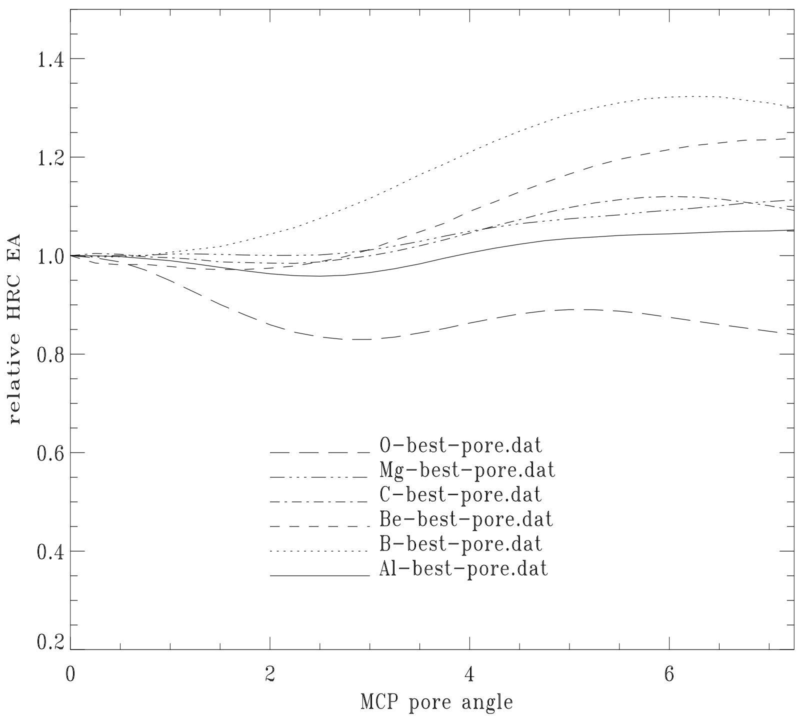

Figure 25: Relative HRC EA with HRMA versus choice of MCP bias angle angle . The measured Philips (HRC-S) type MCP had 6° bias. The measured GEOC (HRC-I) type MCP had a 4.7° bias angle.

the detector QE and EA, as derived from flat field measurements, must be derated. The derating factors have been determined by:

$$QE_{HRMA} : QE_{flat-field} = \frac{\sum_i^4 EA_i < QE_i >}{\sum_i^4 EA_i}$$

$< QE_i >$ is the expected QE of the HRC appropriately averaged over incident angles from the i^{th} HRMA shell.

$$< QE_i(\omega) > = \int_0^{2\pi} QE(\theta_i, \phi) d\phi$$

EA_i is the effective area of the appropriate shell at the energy of interest.

The de-rating factors are presented in Figures 26, 27 and Tables 1, 2. The de-rating factors vary from $\sim 12\%$ to less than 0.1% over the set of energies tested.

HRMA to flat-field derating factors

Energy	Derate factor
108.5	0.959
183.3	0.883
277.0	0.934
524.9	0.996
1253.6	0.999
1486.7	0.995

Table 1: HRMA De-rating factors to convert flat field QE or EA values to corresponding values when HRC-S type 6° bias MCPs are used.

Verifying or checking the derating factors by comparing XRCF determined QE values with flat field determined QE values is problematic as the HRC detectors were modified in the interim period.

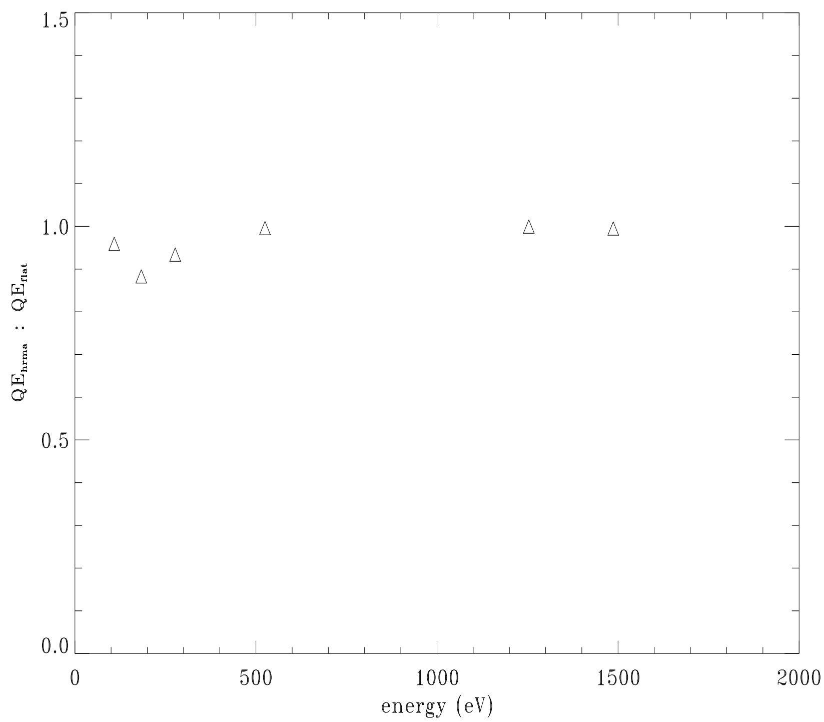

Figure 26: De-rating factors for applying HRC-S flat field data to operation in the converging beam of the HRMA (assuming 6° pore bias).

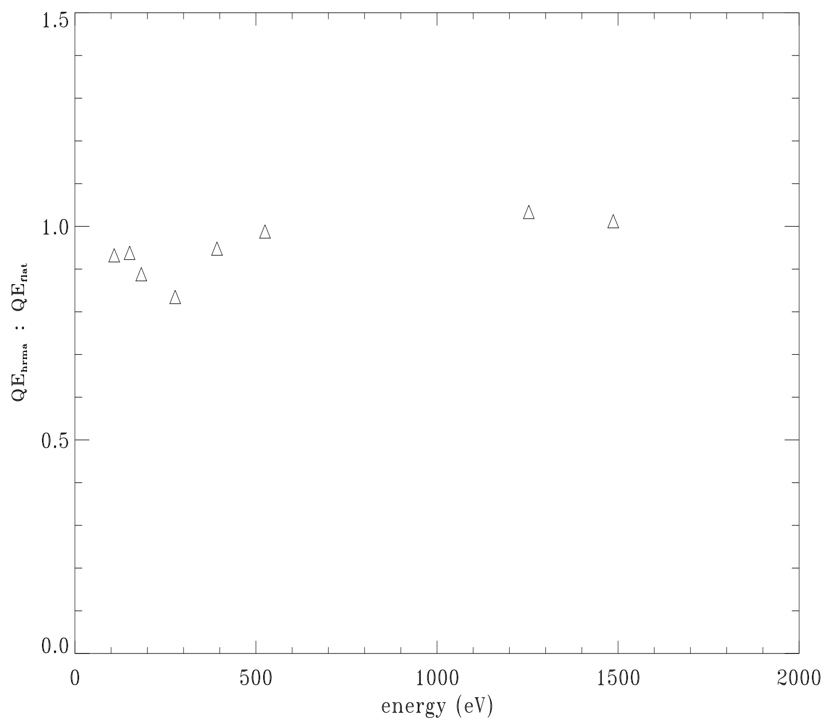

Figure 27: De-rating factors for applying HRC-I flat field data to operation in the converging beam of the HRMA (assuming 4.7° pore bias).

HRMA to flat-field derating factors

Energy	Derate factor
108.5	0.932
151.1	0.938
183.3	0.888
277.0	0.834
392.4	0.947
524.9	0.988
1253.6	1.03
1486.7	1.01

Table 2: HRMA De-rating factors to convert flat field QE or EA values to corresponding values when HRC-I type 4.7° bias MCPs are used.

6 Conclusion and Discussion

Using representative coated MCPs we have measured the relative QE versus X-ray angle of incidence for $\sim$ 10 energies. We have scanned over angles that cover the pertinent AXAF HRMA cone angles. Using this data as representative of the flight detectors, correction factors for flat-field determined QE values to QE values obtained in the converging HRMA beam have been determined.

We have reaffirmed the advantages of using CsI coated MCPs with 6° pore angles to optimize the HRMA/HRC Effective Area, however it is quite probable that the flight GEOC MCPs have only 4.7° bias angles.

The errors in applying these data are primarily systematic; these data were taken with representative MCPs; not the actual flight items CsI coating thicknesses may be different as well as pore angle. Statistical errors have all been kept $\sim$ 3% by appropriate integration times.